c

NOVA V2362 CYGNI (NOVA CYGNI 2006): *SPITZER*, *SWIFT*, AND GROUND-BASED SPECTRAL EVOLUTION

David K. Lynch[1,23], Charles E. Woodward[2,23], Robert Gehrz[2], L. Andrew Helton[2], Richard J. Rudy[1,23], Ray W. Russell[1,23], Richard Pearson[1,23], Catherine C. Venturini[1], S. Mazuk[1], John Rayner[3], Jan-Uwe Ness[4], Sumner Starrfield[4], R. Mark Wagner[5], Julian P. Osborne[6], Kim Page[6], Richard C. Puetter[7], R. Brad Perry[8], Greg Schwarz[9], Karen Vanlandingham[9], John Black[10], Michael Bode[11], Aneurin Evans[12], Thomas Geballe[13], Matthew Greenhouse[14], Peter Hauschildt[15], Joachim Krautter[16], William Liller[17], James Lyke[18], Jim Truran[19], T. Kerr[20], S. P. S. Eyres[21], and Steven N. Shore[22]

[1] The Aerospace Corporation, M2/266, P.O. Box 92957, Los Angeles, CA 90009, USA; david.k.lynch@aero.org, Richard.J.Rudy@aero.org, Ray.Russell@aero.org, Richard.Person@aero.org, Catherine.C.Venturini@aero.org, S.Mazuk@aero.org

[2] Department of Astronomy, School of Physics & Astronomy, 116 Church Street S.E., University of Minnesota, Minneapolis, MN 55455, USA; chelsea@astro.umn.edu, gehrz@astro.umn.edu, ahelton@astro.umn.edu

[3] Institute for Astronomy, 2680 Woodlawn Drive, Honolulu, HI 96822, USA; rayner@ifa.hawaii.edu

[4] School of Earth & Space Exploration, Arizona State University, P.O. Box 871404, AZ 85287-1404, USA; sumner.starrfield@asu.edu, ness@susie.la.asu.edu

[5] Large Binocular Telescope Observatory, 933 North Cherry Avenue, Tucson, AZ 85721, USA; rmw@as.arizona.edu

[6] Department of Astronomy, University of Leicester, University Road, Leicester LE1 7RH, UK; julo@star.le.ac.uk, kpa@star.le.ac.uk

[7] CASS, University of California; San Diego, 9500 Gilman Dr., La Jolla, CA 92093, USA; rpuetter@ucsd.edu

[8] NASA Lark, Hampton, VA 23681, USA; Raleigh.B.Perry@NASA.gov

[9] West Chester University of Pennsylvania, West Chester, PA 19383, USA; gschwarz@pha.jhu.edu, kvanlandingham@wcupa.edu

[10] Onsala Space Observatory, Chalmers University of Technology, Onsala, S-439 92, Sweden; jblack@oso.chalmers.se

[11] Astrophysics Research Institute, Liverpool John Moores University, Twelve Quays House, Birkenhead, CH41 1LD, UK; mfb@astro.livjm.ac.uk

[12] Astrophysics Group, Keele University, Keele, Staffordshire, ST5 5BG, UK; ae@astro.keele.ac.uk

[13] Gemini Observatory, 670 N. A'ohoku Place, Hilo, HI 96720, USA; tgeballe@gemini.edu

[14] NASA Goddard/JWST, Greenbelt, MD 20771, USA; matt.greenhouse@nasa.gov

[15] Hamburger Sternwarte, Universität Hamburg, Gojenbergsweg 112, Germany; yeti@hs.uni-hamburg.de

[16] Landessternwarte, Königstuhl, D-69117 Heidelberg, Germany; j.krautter@lsw.uni-heidelberg.de

[17] U. Chile, Renaca Bajo, Chile; wliller@compuserve.com

[18] Keck Observatory, 65-1120 Mamalahoa Hwy, Kamuela, HI 96743, USA; jlyke@keck.hawaii.edu

[19] Department of Astronomy & Astrophysics, University of Chicago, 5640 S. Ellis Ave., Chicago, IL 60637, USA; truran@nova.uchicago.edu

[20] Joint Astronomy Centre, 660 N. A'ohoku Place, University Park, Hilo, HI 96720, USA; t.kerr@jach.hawaii.edu

[21] Centre for Astrophysics, University of Central Lancashire, Preston, PR1 2HE, UK; spseyres@uclan.ac.uk

[22] Dipartimento di Fisica "Enrico Fermi," Universitá di Pisa; INFN-Sezione di Pisa, Italy; shore@df.unipi.it

ABSTRACT

Nova V2362 Cygni has undergone a number of very unusual changes. Ground-based spectroscopy initially revealed a normal sequence of events: the object faded and its near-infrared emission lines gradually shifted to higher excitation conditions until about day 100 when the optical fading reversed and the object slowly brightened. This was accompanied by a rise in the *Swift* X-ray telescope flux and a sudden shift in excitation of the visible and IR spectrum back to low levels. The new lower excitation spectrum revealed broad line widths and many P-Cygni profiles, all indicative of the ejection of a second shell. Eventually, dust formed, the X-ray brightness—apparently unaffected by dust formation—peaked and then declined, and the object faded at all wavelengths. The *Spitzer* dust spectra revealed a number of solid-state emission features that, at this time, are not identified.

Key words: accretion, accretion disks – line: profiles – novae, cataclysmic variables – stars: winds, outflows

1. INTRODUCTION

Though different in their details, most classical novae (CN) follow a fairly consistent development sequence (Bode & Evans 1989; Hernanz & Jose 2002): a thermonuclear runaway (TNR) on the surface of a white dwarf (WD) in a contact binary system ignites. This happens when material accreted onto the WD from the secondary star reaches a sufficiently high temperature, typically 10^7 K at the base of the accreted material depending on its density. The energy released by the TNR drives a super-Eddington expansion and ejects 10^{-6}–10^{-4} $M_\odot$ of material that expands to form a shell. Light from the shell increases rapidly because of its increasing surface area and in a few hours or days, the CN brightens by 4–5 orders of magnitude. This sudden brightening is the "nova." At maximum brightness, its spectrum resembles that of an F-type star and emission lines appear, some with short-lived P-Cygni profiles, and virtually all due to H I, He I, and neutral metals. The TNR is like a match that lights the surface material. After the initial impulsive ejection, the nova begins to fade even though nuclear burning and the associated stellar winds can continue for months or years after the outburst. As the wind flux decreases, the optical-depth-unity surface recedes, thereby exposing deeper and hotter layers of the WD's expanding photosphere. The increasing UV radiation begins to ionize the neutral species whose emission lines weaken and eventually disappear altogether, except for H I and He I. In due course He II appears, then the nebular lines and, finally, the photo-ionized, collisionally-excited coronal lines emerge to dominate the spectrum. During this time, the nova's brightness fades by many magnitudes and the system eventually reverts to its quiescent, accreting phase.

[23] Visiting Astronomer at the Infrared Telescope Facility, which is operated by the University of Hawaii under Cooperative Agreement no. NCC 5-538 with the National Aeronautics and Space Administration, Science Mission Directorate, Planetary Astronomy Program.

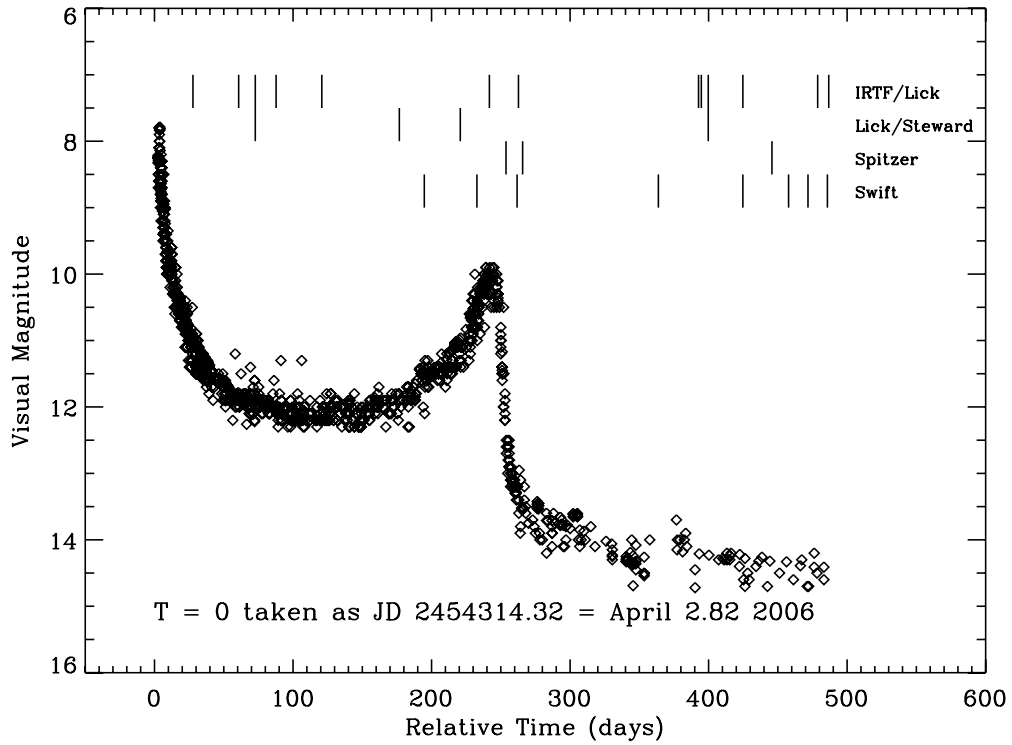

Figure 1. AAVSO visible light curve of V2362 Cygni with dates of observations reported in this paper indicated by vertical lines. The brightness declined normally until about day 150 when it began brightening. Near day 243 (2006 December 1, JD2454071) dust began forming and blocked the visible light leading to a sharp decline in brightness. Day = 0.0 = 2006 April 2.807 = JD 2453828.30750. This light curve is very similar to that of V1493 Aql (Novae Aquilae 1999 #1).

V2362 Cygni was different. At first it behaved according to expectation. Then, while the neutral metal lines were fading and the He I lines were strengthening, the optical decline stopped and the nova brightened again (see the American Association of Variable Star Observers, AAVSO, light curve in Figure 1). This unusual behavior—as we will see from the IR and X-ray observations—probably indicates that after the initial TNR, the nuclear burning did not subside as it does in most novae, but instead strengthened and appeared to produce a second ejection event before shutting down for good.

V2362 Cygni (Nova Cygni 2006) was discovered near maximum light ($m_V \sim 7.5$) by H. Nishimura on April 2.807 UT (Nakano et al. 2006) at coordinates 21 11 32.35 +44 48 03.7 (J2000.0). At first, it appeared to be a CN with t_2 and t_3 being 10.5 and 24 days, respectively, but after about two months of monotonic decline, the light curve flattened, and then the object began to brighten. V2362 Cyg reached a secondary peak of $m_V \approx 9.8$ on around 2006 December 1 (day 243) followed by a precipitous fading that signaled the onset of dust formation. Though evolving somewhat faster, V1493 Aquilae (Nova Aquilae 1999 #1) showed a very similar light curve (Bonifacio et al. 2000; Dobrotka et al. 2006; Venturini et al. 2004). In this paper, we report and analyze visible, IR, and X-ray observations of the nova during its first 500 days and discuss them in the context of possible scenarios.

2. OBSERVATIONS

Our observations began on 2006 April 30 and continued through the summer of 2007. Table 1 lists the data log for the observations reported here. Spectra in the 0.8–5.5 μm range were obtained using SpeX (Rayner et al. 2003) on the NASA Infrared Telescope Facility (IRTF) in the usual single-beam single-nod mode using a 0.8 × 15 arcsec slit and a 7 arcsec nod. Spectral resolution was about 1000. Reductions were done with SpeXTools (Cushing et al. 2004). Similar spectra in the 0.5–2.5 μm region were obtained with the Visible-to-Near-Infrared Imaging Spectrograph (VNIRIS) on the Lick Observatory 120″ telescope using a 2 arcsec slit and nodding by 20 arcsec along the slit to subtract out the background sky. Reduction techniques were standard and have been described in earlier papers, e.g., Rudy et al. (2003). The *Swift* X-Ray Telescope observations were performed in photon counting mode. X-ray telescope (XRT) data were extracted and processed using the standard *Swift* tools[24], specifically xrtpipeline v0.11.3. We used event grades 0–12 and extracted events using a 24 arcsec radius region around the nova (Ness et al. 2007).

2.1. Ground-Based Infrared and Optical Observations

Figures 2 and 3 provide an overview of the IR spectral development of the nova. The first five (top five) IR spectra in Figures 2 and 3 are typical of a CN during its early post-maximum phase. The neutral metal lines weakened and the higher excitation lines strengthened, most notably the He I lines at 1.0830 and 2.0581 μm. The Lyman β-fluoresced O I lines were strong and many lines of C I and N I were also present (see Figures 4 and 5 and Table 2 for line identifications in the 0.8–4.5 μm region). The six unidentified lines that frequently appear in novae at 1.1114, 1.1901, 1.5545, 2.0996, and 2.425 μm (Williams et al. 1996; Lynch et al. 2001, 2004) were not evident. On or immediately after 2006 November 30, dust formed and changed the spectral energy distribution (SED) of the nova shell.

The optical spectra from Steward and Lick are shown in Figure 6 with the line identifications for the earliest spectrum

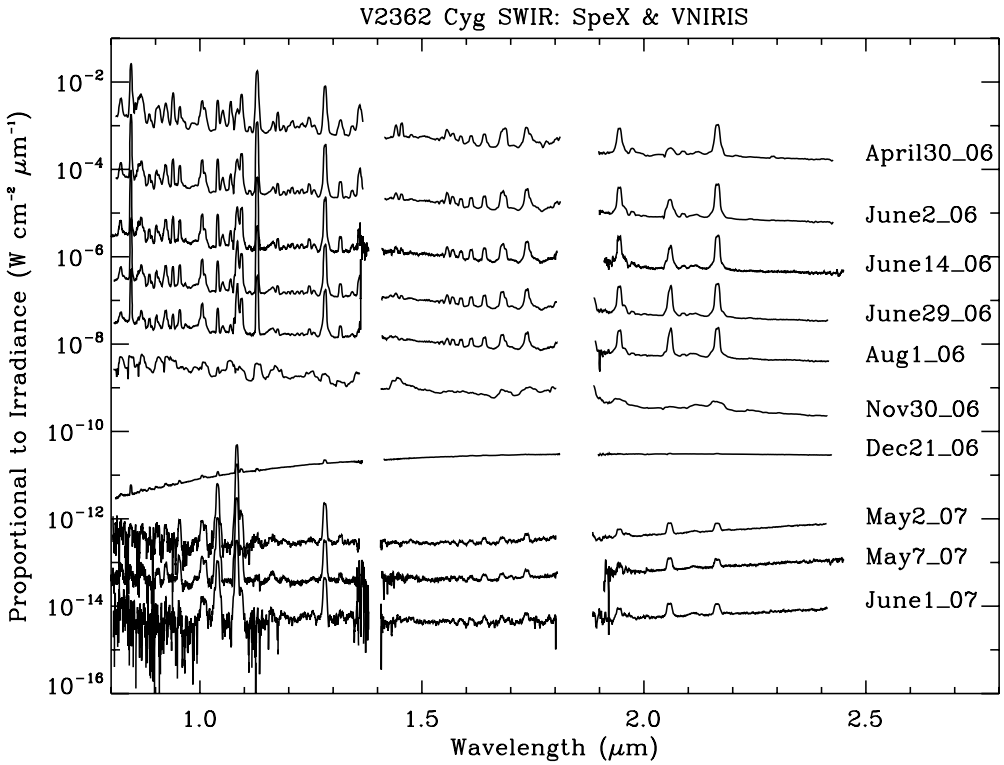

Figure 2. The 0.8–2.5 μm spectral development. The earliest spectrum is on top and the others have been arbitrarily scaled to place them in time-order position downward on the graph. The spectra have been slightly smoothed to suppress noise.

Table 1
Observation Log

Date (UT)	Age (Days)	Telescope	Instrument	Wavelength (μm or keV)	Resolution ($\lambda/\Delta\lambda$)
2006 Apr 30	28	IRTF	SpeX	0.8–5.5 μm	~1000
2006 Jun 02	61	IRTF	SpeX	0.8–5.5 μm	~1000
2006 14 Jun 14	73	Lick 120″	VNIRIS	0.5–2.5 μm	~1000
2006 Jun 29	88	IRTF	SpeX	0.8–5.5 μm	~1000
2006 Aug 01	121	IRTF	SpeX	0.8–5.5 μm	~1000
2006 Sep 26	177	Steward 90″	B&C	0.35–0.7 μm	~1000
2006 Oct 14	195	*Swift*	XRT	0.3–10 keV	Integrated
2006 Nov 09	221	Steward 90″	B&C	0.35–0.7 μm	~1000
2006 Nov 21	233	*Swift*	XRT	0.3–10 keV	Integrated
2006 Nov 30	242	IRTF	SpeX	0.8–5.5 μm	~1000
2006 Dec 12	254	IRTF	BASS	3–14 μm	~100
2006 Dec 12	254	*Spitzer*	IRS	5.2–38 μm	~600
2006 Dec 20	262	*Swift*	XRT	0.3–10 keV	Integrated
2006 Dec 21	263	IRTF	SpeX	0.8–5.5 μm	~1000
2006 Dec 24	266	*Spitzer*	IRS	5.2–38 μm	~600
2007 Apr 18	381	*Swift*	XRT	0.3–10 keV	Integrated
2007 Apr 30	393	IRTF	SpeX	2.3–5.5 μm	~1000
2007 May 02	395	IRTF	SpeX	0.8–2.5 μm	~1000
2007 May 07	400	Lick 120″	VNIRIS	0.5–2.5 μm	~1000
2007 Jun 01	425	IRTF	SpeX	0.8–5.5 μm	~1000
2007 Jun 20	444	*Swift*	XRT	0.3–10 keV	Integrated
2007 Jun 22	446	*Spitzer*	IRS	5.2–38 μm	~600
2007 Jul 04	458	*Swift*	XRT	0.3–10 keV	Integrated
2007 Jul 18	472	*Swift*	XRT	0.3–10 keV	Integrated
2007 Jul 25	479	IRTF	SpeX	0.8–5.5 μm	~1000
2007 Aug 01	486	*Swift*	XRT	0.3–10 keV	Integrated

(2006 June 14) given in Table 3. During the first six months, the spectrum was characteristic of a low-excitation spectrum and it changed slowly. The main developments involved the strengthening and weakening of various lines as the object entered its early nebular phase in the spring and summer of 2006 and then reverted to a low-excitation stage in the autumn of 2006. The N II line blend at 5676 and 5680 Å and the as yet unidentified line complex at 7210 Å strengthened dramatically. The [O III]

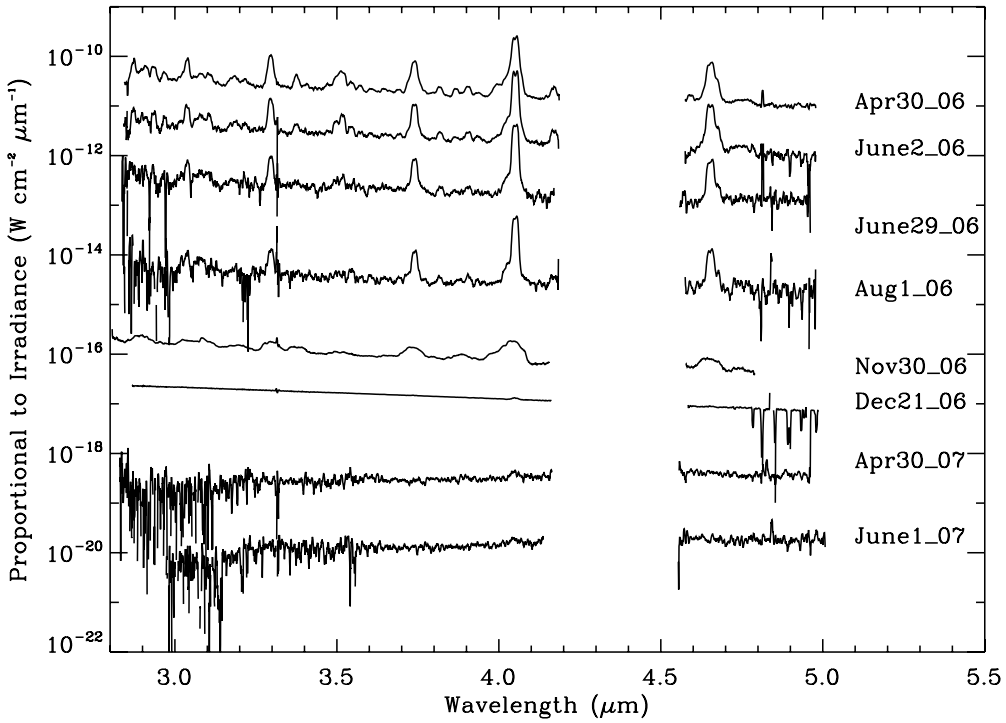

Figure 3. The 2.8–5.0 μm spectral development. The earliest spectrum is on top and the others have been arbitrarily scaled to place them in time-order position downward on the graph. The spectra have been slightly smoothed to suppress noise. All the features longward of 4.6 μm are probably questionable due to the spectrum's low signal-to-noise ratio (S/N).

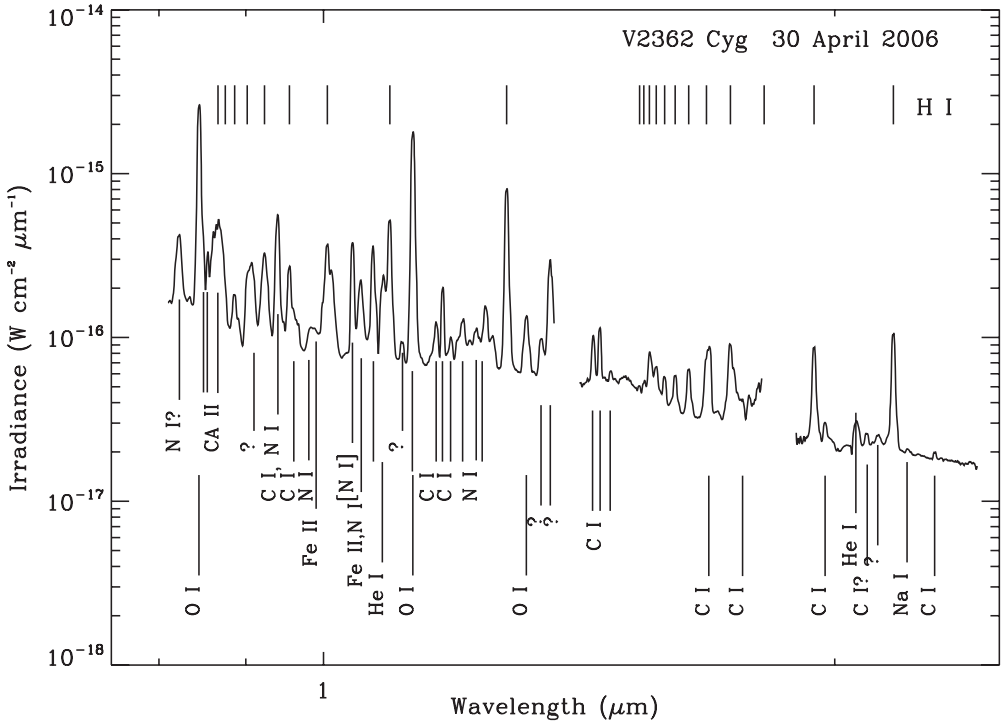

Figure 4. Line identifications for the 0.8–2.3 μm region for 2006 April 30. These lines are the characteristic of the lines in all of the short-wave infrared (SWIR) spectra (Figure 2). The H I lines are indicated by short vertical lines above the spectrum. He I and heavy elements are shown below the spectrum.

doublet at 4959 and 5007 Å slowly strengthened but by 2006 November had disappeared as the spectrum rejuvenated. Also evident in the 2006 November 9 spectrum are P-Cygni profiles from the second outburst.

The line profiles showed evidence of a doubling that is suggestive of a bilobed asymmetrical expansion (Figures 7 and 8). Full width at half-maximum (FWHM) intensity of the lines was about 1300 km s^{-1} with a separation of the two velocity components of approximately 470 km s^{-1}. Between the initial outburst and 2006 August 1, the line profiles remained about the same width. The Steward Observatory optical spectra of 2006 September 26 and 2006 November 9 (Figure 6 and Table 3) revealed line widths that were about 1830 and 3700 km s^{-1} respectively, indicating a rapid broadening of the lines. The

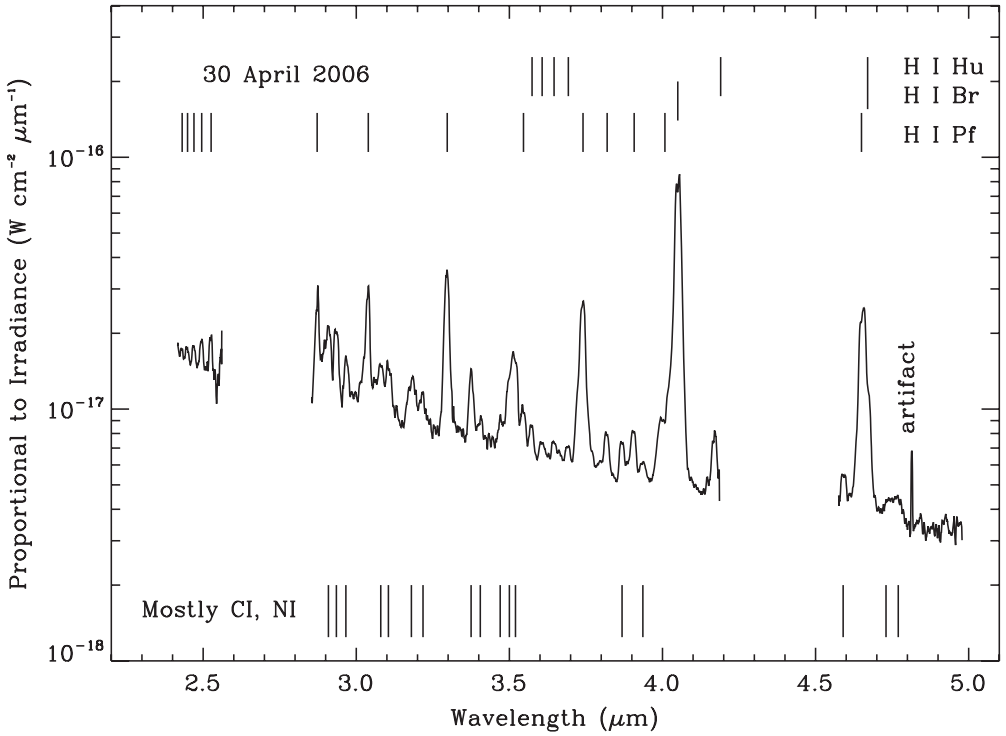

Figure 5. Line identifications for the 2.4–5.0 μm region for 2006 April 30. These lines are characteristic of the lines in all of the MWIR spectra (Figure 3). The H I lines are indicated by short vertical lines above the spectrum. He I and heavy elements are shown below the spectrum. All the features longward of 4.6 μm are probably questionable due to the spectrum's low S/N.

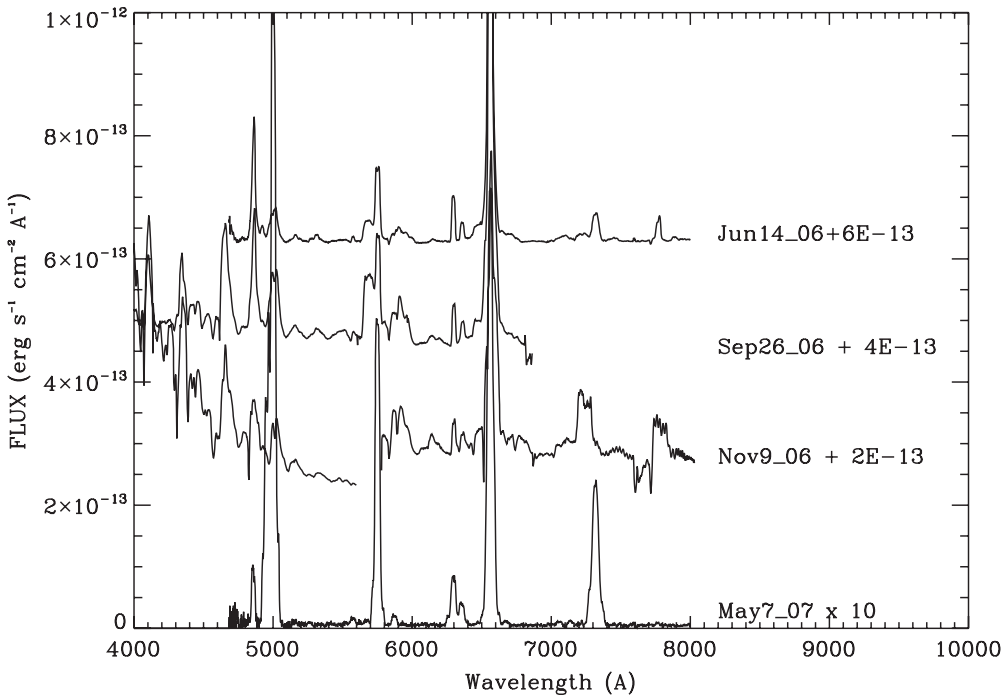

Figure 6. The optical spectral development. The dates are followed by the amount by which the spectrum has been shifted so that they do not fall on the other spectra and thus can be seen more clearly.

profiles on November 30 were markedly different from the others; with a FWHM of 3500 km s^{-1} and a redshift of 200 km s^{-1}, the line profiles on November 30 did not resemble the profiles of the earlier or later spectra. After dust had formed, the FWHM of the line profiles reverted to 1700 km s^{-1} (Figure 9).

Figure 10 shows spectra of V2362 Cyg before and after dust formed. The change in such a short time is remarkable. The dust blocked most of the visible light and produced thermal emission. The emission peaked around 2.05 μm, corresponding to a temperature of 1410 $\pm$ 15 K, the hottest dust ever observed in a CN outburst and very close to its condensation temperature, probably around 1500 K assuming normal abundances of heavy elements. The spectrum also fits a Planck function very closely, which suggests that it was optically thick and

Table 2
Line Identifications for Figures 2 and 3

Measured Wavelength or Vacuum (μm)	Line Identification and Notes
0.8180	Weak—on wing of next line
0.8225	Mg II?
0.8334	C I? Weak
0.8446	O I
0.8500	Weak, red wing of O I probably Ca II & Pa 16
0.8550	Weak Ca II & Pa 15
0.8611	Blended with next two Pa 14?
0.8648	Blended Ca II Pa 13?
0.8673	Blend extending to 0.877
0.8860	
0.8909	Weak
0.9025	Weak, blended Pa 10
0.9070	[S III]?
0.9230	Pa 9
0.9271	Weak
0.9398	C I, N I
0.9546	Pa epsilon
0.9605	Weak C I
0.9655	Weak
0.9803	Weak, blended N I
0.9900	Weak, blended
0.985	Weak, broad blend
0.9998	Fe II 0.9998
1.0040	Pa delta
1.0100	C I, N I
1.0400	[N I]
1.0521	Fe II 1.0500, N I
1.0692	C I
1.0811	He I with blue blend Fe II?
1.0847	Weak. Blend?
1.0938	Pa gamma
1.1125	Fe II 1.1126
1.1281	O I 1.1287
1.1647	C I
1.1751	C I
1.1882	Weak C I
1.2000	Weak
1.2070	N I
1.2196	
1.2289	N I weak
1.2310	
1.2458	N I ?
1.2580	C I
1.2819	Pa beta
1.3104	Weak blended with next line
1.3168	O I? N I
1.3223	Weak blended with previous line
1.3433	N I
1.3600	N I complex
1.4414	C I
1.4542	C I
1.4761	C I
1.55	Blend of weak lines
1.5343	Br 18
1.5439	Br 17
1.5560	Br 16
1.5695	Br 15
1.5880	Br 14
1.6108	Br 13
1.6409	Br 12
1.6812	Br 11 blended with next
1.6863	Fe II blended with previous
1.7090	Weak Mg I?
1.7356	Br 10
1.7433	Fe II blended with previous on red wing

Table 2
(Continued)

Measured Wavelength or Vacuum (μm)	Line Identification and Notes
1.7550	Fe II weak, blended
1.7642	Fe II weak, blended
1.7806	O I? C I
1.7928	Weak
1.9446	Br epsilon
1.9748	Fe II
2.0602	He I with P Cygni +Fe II
2.0890	Fe II
2.1066	Weak
2.1201	Weak
2.1653	Br gamma
2.2060	Weak Na I?
2.2903	Weak C I
2.31	Weak
2.4314	Pf 15
2.4490	Pf 14
2.4699	Pf 13
2.4952	Pf 12
2.625	Atmosphere? Pf theta
2.8718	Atmosphere? Pf 11-5
2.9106	
2.9339	
2.9667	
3.0374	Pf epsilon
3.0800	Weak, blend
3.1074	Weak, blend
3.1838	Weak, blend
3.2155	Weak, blend
3.2957	Pf delta and weak blend
3.3700	Blend
3.4050	Weak probably Hu line
3.4975	Blended with next line
3.5190	Blended with previous line
3.5458	Hu 18 22-6
3.5718	Weak
3.6066	Hu 12 18-6 blend
3.6455	Weak, blend
3.7394	PF 8-5
3.8180	Hu 10 16-10
3.8680	
3.9050	Weak Hu 9 15-6
3.9948	
4.0200	HU 8 14-6
4.0511	Br alpha
4.1700	Hu 7 weak, blend?
4.6536	Pf beta 2
4.6753	Hu epsilon 5 weak, blended with Pf beta 2

lacked any significant spectral structure that could indicate dust composition.

The date of dust formation is unknown but is certain to have occurred between 2006 November 30 and December 12. On the former date, there was no evidence of thermal emission from dust, while on the latter date, the thermal emission was detected at longer wavelengths (Lynch et al. 2006) but was not immediately recognized as being due to dust: the dust's high temperature produced a Rayleigh–Jeans spectrum in the 3–14 μm range whose shape was indistinguishable from that of a gaseous photosphere.

2.2. Spitzer Space Telescope Data

Figure 11 shows the *Spitzer Space Telescope* spectra of the object on 2006 December 12 and 2006 December 24 (days

Table 3
Line Identifications for Figure 6

Measured Wavelength or Vacuum (Å)	Line Identification and Notes
4015	Weak He I? 4026
4058	O II? N II? 4041
4102	Broad, P-Cygni? H I 6–2?
4307	Weak O II? 4294
4340	Blended with next H I 5–3 4340
4365	Blended with previous Fe II? [O III]? 4363
4462	He I 4471?
4530	Broad, blend Fe II
4596	Weak, broad Fe II? 4596, 4583
4640	Blended with next—P-Cygni? O II? 4607 C III? 4640 N III? 4640
4657	Blended with previous O II? 4651
4688	Weak, blended with previous He II? 4686
4780	Weak
4865	H I 4-2 4859
4895	Weak, blended with previous
4923	Weak Fe II? 4924 He I? 4922
4970	Weak, blended with next [O III]? 4959?
4995	Fe II? [O III]? 4959?
5023	Fe II He I? 5015 N II? 5005 [O III] 5007 Fe II? 5018
5157	Center of broad blend Mg I? Fe II? N II? [Fe VI]? 5176
5202	Weak, red wing of previous Mg I? Fe II?
5272	Weak Fe II? 5276
5310	Center of broad blend Fe II? 5317
5458	Center of broad blend
5575	[O I]? 5577
5690	Center of blend of the N II lines at 5676 & 5680
5752	N II 5755
5870	Center of blend of two lines He I? 5876
5910	Fe II
5967	
6139	Center of broad blend O I?
6195	Weak
6310	[O I]? 6300
6368	Fe II? [O I]? 6364
6522	Weak, on blue wing of H I
6563	H I 3–2
6603	Weak, on red wing of H I [N II]? 6584
6703	He I? 6678 weak, blend
6758	Weak, blend
7035	He I? 7065 blended with next, weak
7100	He I? 7065 bended with previous, weak
7210	Weak, blend?
7260	Strong
7320	He I? Fe II? & [O II]? several
7470	Weak N I? 7468 Fe II? two
7599	Weak, narrow He II? 7593
7774	O I 7774
7880	

254 and 266, respectively). The first spectrum was probably taken during the early stages of dust formation and the second about 12 days later when there was abundant dust. In the second spectrum, the H I lines are almost completely obscured although the [O IV] line was not blocked and appeared to have strengthened. The two spectra show no evidence of solid-state dust features (e.g., silicates), which is probably the result of the dust shell being optically thick. As the shell expanded, the dust absorption decreased until it became sufficiently optically thin to reveal a spectral structure due to dust emission. Figure 12 shows the *Spitzer* spectrum for 2007 June 22 (day 479) and reveals emission lines of [Ne II], [Ne III], [Ne V], and [O IV]. It also showed broad dust emission features at 6.4, 8.05, 11.3, and ∼18 μm, the interpretation of which is discussed in Section 5 below.

Table 4
Swift XRT Light Curve

Day	Expos (ks)	Rate (0.3–10 keV) ($c\ s^{-1}$)	HR $(H-S)/(H+S)$
194.29	2.3	0.0112 ± 0.0020	$0.35 + 0.24/-0.18$
231.12	2.6	0.0101 ± 0.0020	$0.50 + 0.19/-0.14$
231.25	4.7	0.0155 ± 0.0018	$0.27 + 0.12/-0.11$
260.98	3.8	0.0206 ± 0.0023	$0.07 + 0.11/-0.13$
379.62	5.2	0.0420 ± 0.0027	$0.11 + 0.07/-0.07$
442.14	2.0	0.0263 ± 0.0035	$0.10 + 0.14/-0.14$
456.40	1.5	0.0225 ± 0.0037	$-0.14 + 0.17/-0.19$
470.34	2.5	0.0160 ± 0.0025	$-0.03 + 0.16/-0.18$
484.92	1.8	0.0207 ± 0.0028	$0.04 + 0.20/-0.19$

Note. Day 0.0 = 2.807 2006 April. HR uses bands 0.3–1.0 and 1.0–10 keV. Baysian errors on HR derived using Kraft et al. (1991).

2.3. Swift X-Ray Telescope Observations

We obtained nine X-ray observations with the *Swift* XRT (Burrows et al. 2005) using a 24 arcsec radius around the object. In Table 4 we list the observation day, exposure time, count rate, and hardness ratio. The count rates were obtained as described in the Appendix in Ness et al. (2007). We also extracted spectra from the recorded photon energies; however, the number of photons was insufficient to obtain a well exposed spectrum. They were, however, good enough to reveal that none of the spectra displayed a Super Soft X-ray Source (SSS) spectrum. An SSS would have indicated that the photosphere of the shell surrounding the WD had receded to a depth where we could detect the underlying WD. SSS spectra usually display a spectrum that resembles a blackbody with temperature ∼50 eV (e.g., Kahabka & van den Heuvel 1997).

Individual observations recorded less than 200 counts each and are thus not suitable for spectral fitting. The hardness ratio values are generally consistent with cosmically abundant optically thin emission at temperatures in the range ∼0.5–1 keV (assuming $N_{\rm H} = 3 \times 10^{21}$ cm^{-2}, as derived from $E(B-V) = 0.58$). We accumulated a spectrum from the entire set of observations; flux is detected up to 4 keV. We were not able to find a good fit using a single-temperature optically thin spectral model. A two-temperature model was a more reasonable fit although this was still poor ($kT_1 = 0.19 \pm 0.02$ keV, $kT_2 = 1.8 \pm 0.2$ keV, $\chi^2 = 2.1$). We were able to obtain a good spectral fit ($\chi^2 = 1.2$) only by the *ad hoc* addition of emission line components from hydrogen-like sodium ($E = 1.23$ keV, EW = 200 eV) and helium-like aluminum ($E = 1.60$ keV, EW = 260 eV). There is no evidence of an SSS optically thick spectral component. For all fits, $N_{\rm H}$ was fixed at the value above, and fits with $N_{\rm H}$ that were allowed to vary gave consistent values. They are consistent with those from XMM-Newton on day 398 given by Hernanz et al. (2007) who reported a flux that was a factor two times higher than our highest XRT value. The X-ray hardness ratio shows only modest evidence for spectral evolution at best.

Figure 13 shows the *Swift* XRT flux in the 0.3–10 keV band as a function of time. For comparison, we have overplotted the scaled visible brightness derived from Figure 1. Although we have no *Swift* data before day 195, it is possible that the upturn in visible brightness was more-or-less co-temporal with the increase in the X-ray flux. How these two events are related is

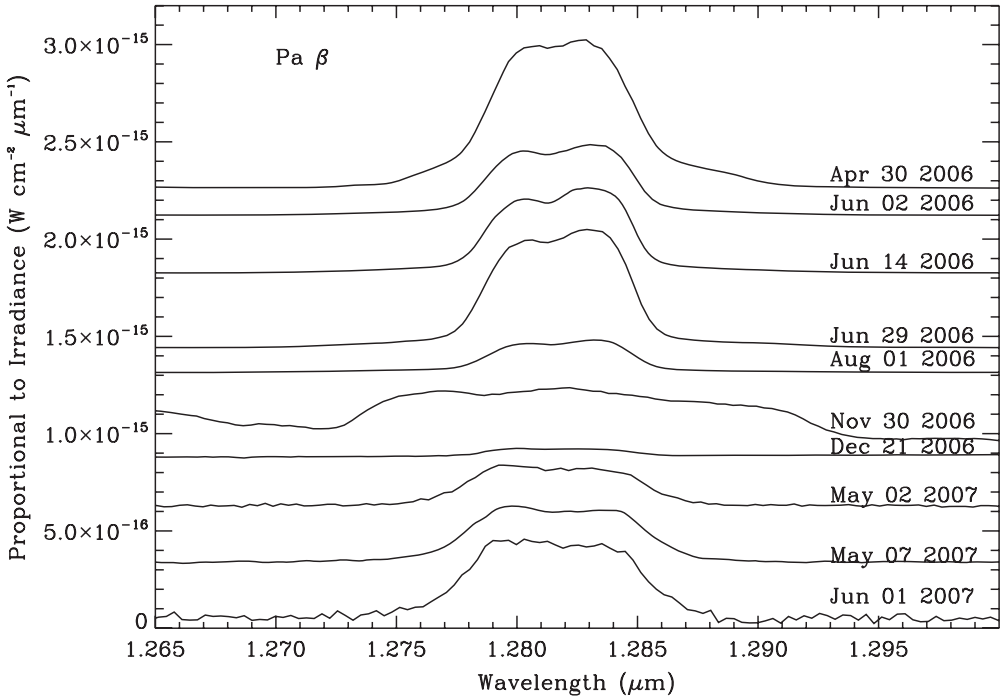

Figure 7. Until about 2006 August, the line profiles had a more-or-less constant shape and FWHM of 1300 km s^{-1}. Between 2006 August and November, the line widths broadened (see Figures 6 and 9) reaching a maximum on or about November 30 with a FWHM of 3500 km s^{-1} and a redshift of about 200 km s^{-1}. After dust formed in early 2006 December, the shapes and widths reverted to their pre-dust conditions. The individual spectra have been vertically scaled and shifted for clarity. There is no line flux information in this plot.

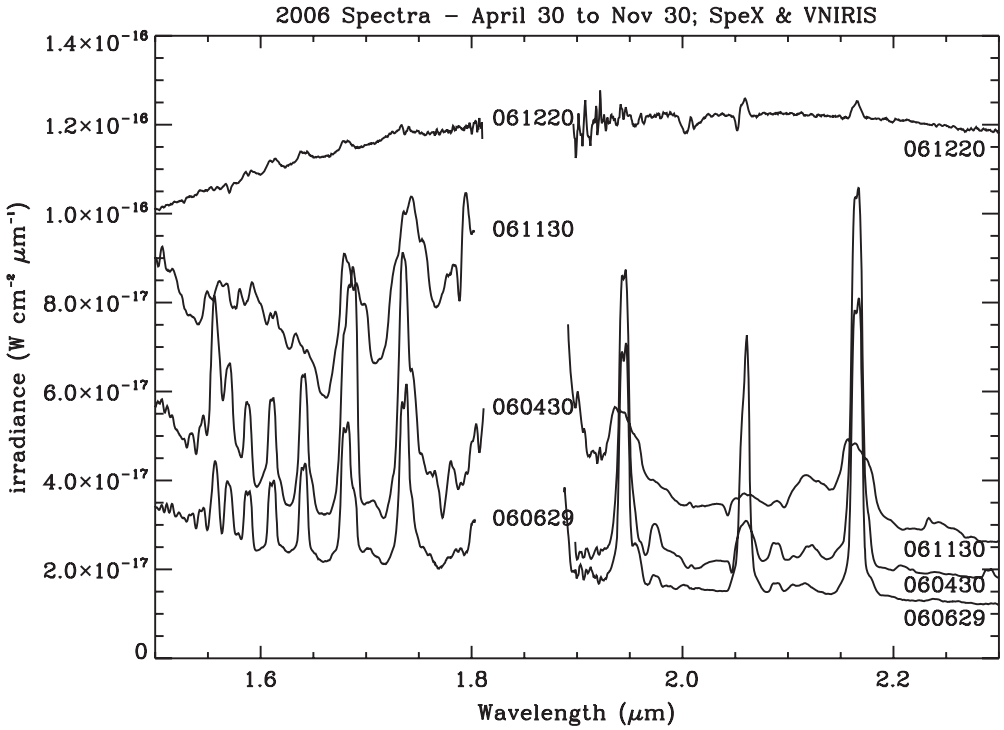

Figure 8. Spectra on April 30, June 29, November 30, and December 20 (a subset of Figure 2). Note the early P-Cygni profiles on the He I 2.0581 μm line that faded as the excitation (and line) grew. The P-Cygni profile had disappeared by June 29 only to appear again with the emergence of the second shell as shown in the December 20 spectrum. The vertical locations have been slightly adjusted to aid visibility.

unclear. The fact that dust formation did not seem to have any effect on the X-ray flux might suggest that the X-ray source was outside of the dust shell, unless the dust's X-ray opacity was low.

3. REDDENING, EXTINCTION, AND DISTANCE

Reddening can be obtained from our spectra using the Lyman β fluoresced O I lines (Rudy et al. 1991). From April to June, the

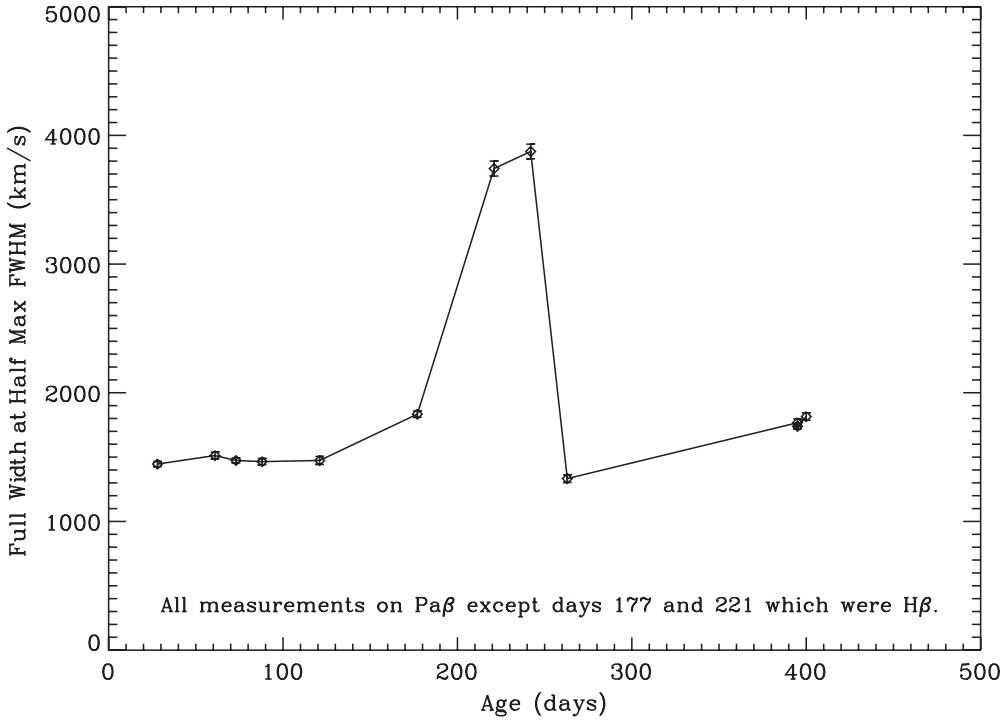

Figure 9. FWHM intensity above the continuum of the H I lines. The line widths remained relatively constant until the beginning of the second ejection event when they broadened with the expulsion of the second shell. After dust formed, the line width declined sharply and returned to roughly their early values.

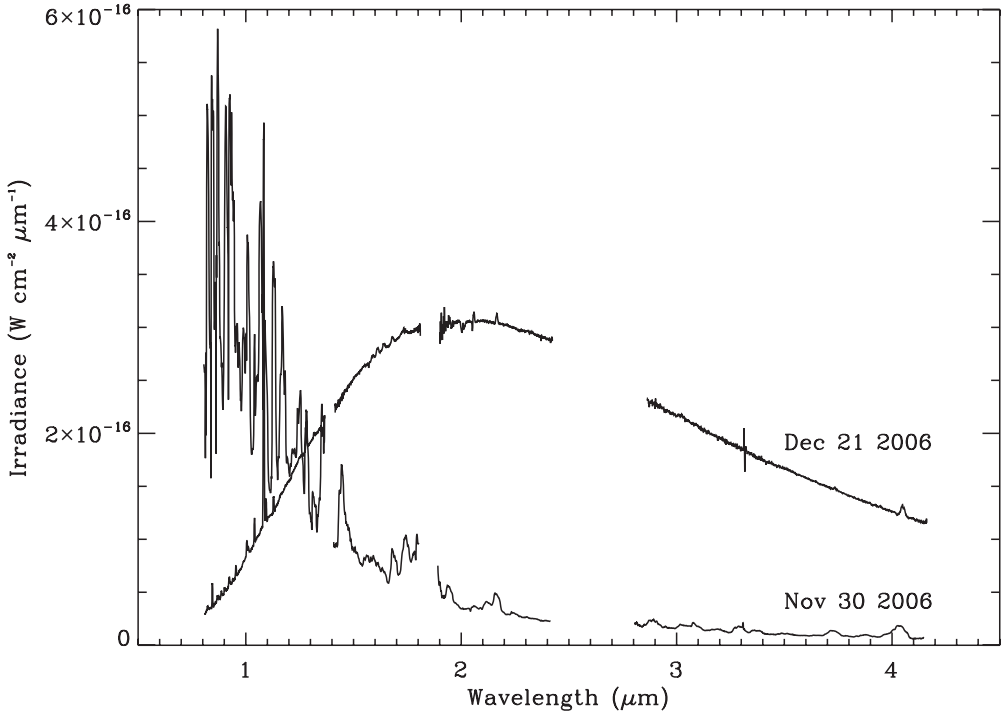

Figure 10. SpeX spectra of V2362 Cyg before and after dust formed. The emission peaked around 2.05 μm corresponding to a temperature of 1410 $\pm$ 15 K. The feature at 3.31 μm is a reduction artifact.

reddening measurements were consistent at $E(B-V) = 0.58 \pm 0.04$. Starting in 2006 August, the emergence of P-Cygni profiles and the broadening of the lines made determinations of the reddening difficult (see Figure 14 and the accompanying explanation below in Section 4). There was some indication of increased obscuration with $E(B-V) = 0.73 \pm 0.11$ on August 1 and $E(B-V) = 0.97 \pm 0.08$ on December 20 (Russell et al. 2006; Mazuk et al. 2006), but the uncertainties are too large to reliably confirm an increased extinction. Adopting $E(B-V) = 0.58 \pm 0.04$ and $A_V/E(B-V) = 3.05$, we find an optical extinction of 1.77 ± 0.12 mag. These numbers are entirely consistent with those reported by Steeghs et al. (2006). Based

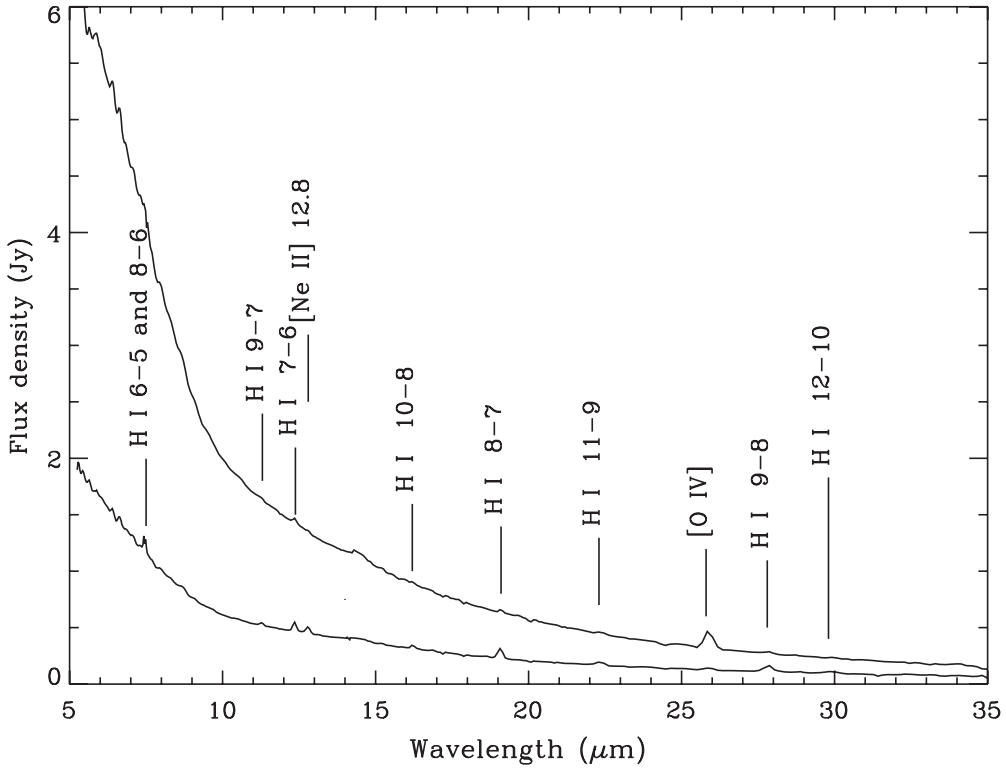

Figure 11. The 5–35 μm spectral development observed by *Spitzer Space Telescope*. As dust formed in early 2006 December, the spectrum brightened significantly while remaining essentially the same shape because this part of the spectrum is on the Rayleigh–Jeans tail of a roughly 1400 K blackbody. Note that dust blocked the H I emission but not the [O IV] emission. The short vertical line at 14 μm between the two spectra is characteristic of 1 standard deviation throughout the spectrum. One standard deviation is about 0.03 Jy.

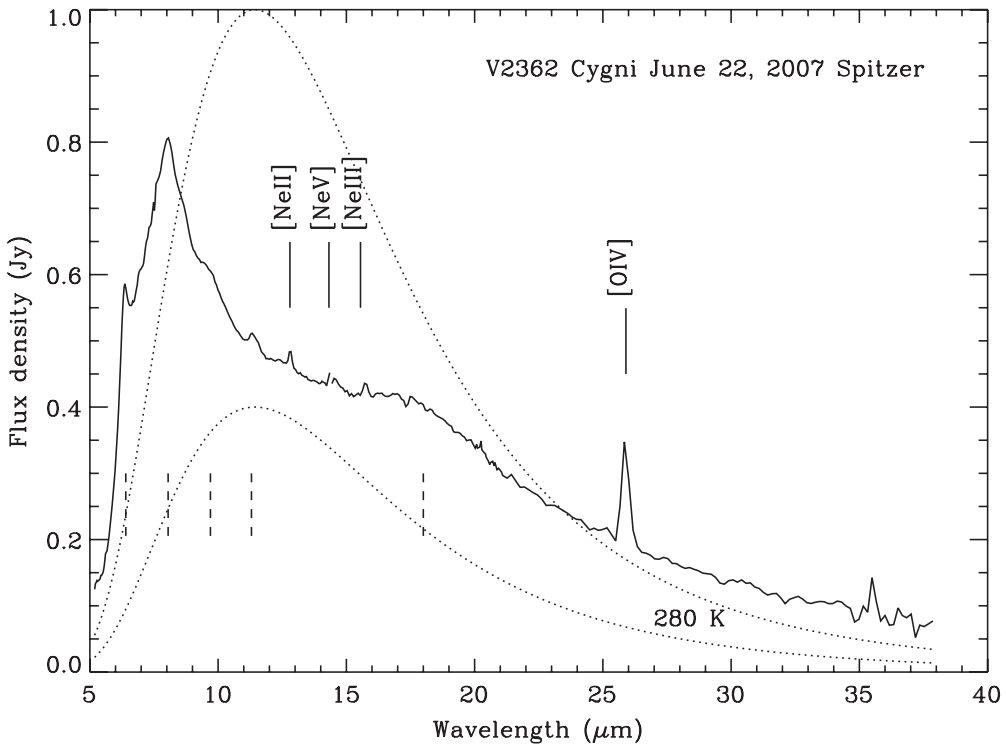

Figure 12. *Spitzer* spectrum of V2362 Cyg on 2007 June 22. The overall shape of the spectrum is extremely non-Planckian, as the two 280 K blackbody functions (dotted curves, differently scaled) show. The identifiable atomic emission lines are [Ne II] 12.8 μm, [Ne V] 14.32 μm, [Ne III] 15.55 μm, and [O IV] 25.98 μm. What seem to be dust emission features (vertical dashed lines) are at 6.37, 8.05, 11.32 μm and a broad one from 15–21 μm.

on the methods of Della Valle & Livio (1995), Buscombe & de Vaucouleurs (1955), and Bonifacio et al. (2000), Kimeswinger et al. (2008) used the above reddening values to derive a distance of 7.5 +3.0 −0.25 kpc, a number that we have adopted here. For a mean XRT count rate of 0.023 counts s^{-1}, the 0.3–10 keV unabsorbed flux (total) = 2.47 × 10^{-12} erg cm^{-2} s^{-1} [lower

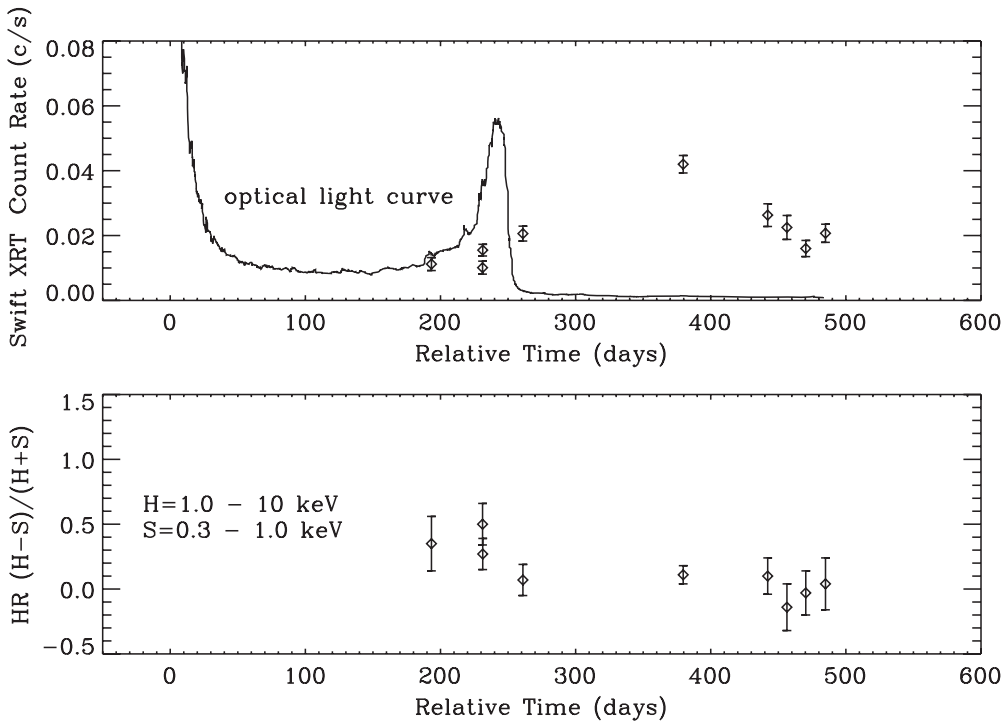

Figure 13. (upper) *Swift* XRT flux in counts s^{-1} for the 0.3–10 keV interval as a function of time (diamonds with $\pm$ 1σ error bars) along with the arbitrarily scaled visible light curve (solid line) from Figure 1 for comparison. Note that the beginning of the upturn in the secondary visible peak roughly coincides with the rise in the *Swift* X-ray flux around day 150. It seems likely that the visible brightness would have continued to rise if dust had not formed and blocked the light. (lower) Hardness ratio of XRT for the observation dates. Though the formal uncertainties are large, there may be a slight trend toward softening of the spectrum.

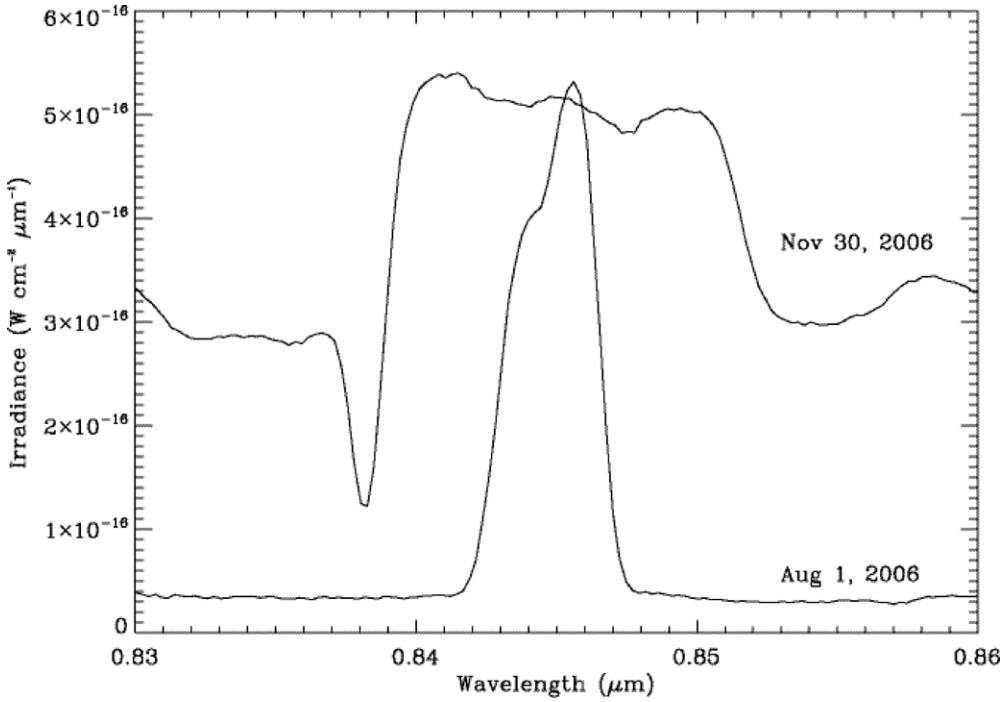

Figure 14. The spectral region around the O I 0.8446 μm on 2006 August 1 and November 30. During the initial decline (2006 August 1), the O I lines remained narrow and relatively well isolated with little spectral structure apart from a slight doubling asymmetry indicative of a bilobed flow. Four months later on 2006 November 30, the line had grown much more complex: it broadened from 1200 to 4250 km s^{-1}, showed evidence of three velocity components, and had developed a P-Cygni profile with a narrow (320 km/s) blueshifted (2270 km s^{-1}) absorption feature. Also note that the continuum brightened by about a factor of eight between August 1 and November 30.

temp = 1.79×10^{-12}, higher temp = 6.05×10^{-13}]. The bolometric (0.001–100 keV) flux would be 9.26×10^{-12} erg cm^{-2} s^{-1}, corresponding to a bolometric X-ray luminosity of $L = 6 \times 10^{34}$ D^2 erg s^{-1} where D is the distance in kpc, D being 7.5 kpc in this case.

4. THE REBRIGHTENING

One interesting aspect of V2362 Cyg was its rebrightening (Figure 1) and spectral rejuvenation (Figures 2, 3, and 6). In view of the large expansion velocity (Figure 9), the optical

Properties of the Nova	Value, Condition or Event
Discovery	2006 Apr 2.807 = JD 2453828.30750
WD type	CO?
R.A. & decl.	21 11 32.35 + 44 48 03.7 (J2000.0)
Galactic lat & long	$l = -2.36$ $b = 87.37$
Peak brightness	$m_V = 7.6$ on 2006 April 2.807
Speed class	Fast, or very fast: $t_2 \approx 10.5$ days and $t_3 \approx 24$ days
Reddening	$E(B-V) = 0.58 \pm 0.04$
Distance	$7.5^{+3.0}_{-0.25}$ kpc (after Kimeswenger et al. 2008)
Speed, 1st ejection	$\sim$1300 km s^{-1}
Speed, 2nd ejection	$\sim$3500 km s^{-1}
Dust	Inexplicable composition

Time Sequence

Date	Day	Event
2006 Apr 2	0	Nova discovered near peak brightness
2006 Jun	$\sim$60	Excitation in the ejecta increasing
$\sim$2006 Jul 10	100	Ejection of second shell, optical brightness leveled off, lines begin to broaden
$\sim$2006 Sep 26	150	P-Cygni profiles developed and strengthened through Nov
$\sim$2006 Nov	200	Spectrum reverted to low excitation, line profiles reverted to original width
2006 Dec	243	Dust formed, brightness decreased sharply, profiles reverted to early width & shape, P-Cygni profiles declining
$\sim$2007 Mar 24	350	X-ray flux peaked (based on 0.3–10 keV measurements)
2007 Mar–Oct	$>$350	Excitation increases, no coronal lines, nova fades

brightening (Figures 1 and 14), and the time behavior of the XRT measurements (Figure 13), it appears that something happened to increase the X-ray luminosity. As noted earlier, the formation of dust did not seem to affect the X-ray light curve.

Some measure of the nova's unusual behavior is revealed in Figure 14, which shows the spectral region around the O I 0.8446 μm line on 2006 August 1 and November 30. The line broadened enormously and grew more complex with the appearance of several velocity components and a narrow P-Cygni absorption component. The continuum level also rose by about a factor of eight. As early as 2006 September 26, the 4640 Å line showed a weak P-Cygni profile and by November 11, most of the Balmer lines also showed such profiles. On December 20 right after dust formed, the He I 2.0581 μm showed a P-Cygni profile but the H I lines did not. After 2006 December 20, no P-Cygni profiles were seen. This behavior appears to indicate the ejection of a shell of material that was moving much faster than the original ejecta.

5. DUST

At 1410 K, the observed dust on 2006 December 20 (Figure 10) was some of the hottest ever seen in an astronomical source. The spectrum was also a near-perfect fit to a blackbody, suggesting that the dust was nearly isothermal, and possibly optically thick. The dust was also optically thick, as Figure 1 shows by the deep drop in optical brightness. The latest *Spitzer* spectrum (Figure 12) obtained on 2007 June 22 shows obvious solid-state emission features at 6.37, 8.05, 11.32, and $\sim$18 μm. Figure 12 also shows that the spectrum was highly non-Planckian. Any attempt to fit a blackbody to the spectrum fell far short of a satisfactory match. The presence of a non-Planckian spectrum indicates three conditions: (1) the dust shell or cloud is probably optically thin, (2) the dust particles are small enough to be optically thin ($\sim$micron size), and (3) the dust particles have significant variation in emissivity and thus are able to reveal spectral features that are indicative of their composition.

The spectrum in Figure 12 is somewhat puzzling because none of the features can be readily identified with the usual features found in dust: silicates, unidentified infrared (UIR; Gillett et al. 1973) or polycyclic aromatic hydrocorbon (PAH; Allamandola et al. 1985) bands, etc. The feature at 11.3 μm—or one very much like it—occurs in both oxygen-rich dust (olivine feature) and carbon-rich dust (UIR bands and some PAH features), though the common wavelength between the two is a coincidence. The broad feature between 18 and 22 μm is suggestive of silicate emission. The absence of a stronger feature near 9.7 μm, however, probably rules out silicates, at least in the way we have come to understand them in comets and oxygen-rich circumstellar dust shells. Similarly, the absence of a complete suite of UIR bands (3.29, 6.2, 7.6/7.7, 8.6, 11.3, and 12.7 μm) suggests that we are not dealing with UIR bands. The very presence of dust emission features probably rules out graphite as a possibility. It is tempting to assign the 6.37 μm feature and 11.3 μm features to $CaCO_3$ (calcite) because it has these two bands in roughly the right strengths and wavelengths, but calcite's strong 14 μm feature is missing.

The most striking feature in Figure 12 is the large broad emission band that peaks at 8.05 μm. Buss et al. (1991) report an 8 μm feature in some carbon stars such as HD 38218 but their spectra also show a broad SiC feature at 11.3 μm, much wider than the weak narrow one that we observed. Sloan et al. (2007) show spectra of a number of C stars and one of them—HD 100764—displays three very weak emission features centered at 6.35, 8.1, and 11.4 μm, tantalizingly close to V2362 Cyg's. They attribute these to PAHs, whose peak wavelength of the features shifts as a function of effective temperature of the exciting star.

With no satisfactory identification of any of the emission features in V2362 Cyg's *Spitzer* spectrum of 2007 June 22, we are left with a mystery. That the emission is due to solid particles seems unequivocal. The spectrum does not even remotely match any of the thousands of astronomical or laboratory spectra we have examined. The closest resemblance is to certain C-rich sources, but even then, the spectra are so different

that we cannot claim that V2362 Cyg's ejecta were C-rich. It is possible and perhaps likely that we are seeing either a heretofore unrecognized excitation/emission process in ordinary dust, or emission from dust with a highly unusual composition.

Could the second ejection have somehow triggered dust formation? If we assume that both brightenings were associated with ejected material that expanded at constant velocity (here taken as 1300 and 3500 km s^{-1}, respectively), then the second shell would have overtaken the first shell on about day 243 when dust formed, providing that the second ejection was launched on day 150. Extrapolating back in time from the optical and X-ray data, we estimate that the second ejection began somewhat earlier, around day 100 (given our infrequent observations, it could have begun as early as days 45–60 as Kimeswenger et al. 2008 suggest). The shells would not be expected to be infinitely thin hollow spheres; they have finite wall thicknesses as a result of the duration of the ejection and subsequent winds. Also, little is known about the density of either shell at the time that the two began to interact. Therefore, it is possible that the second shell triggered shock-induced dust formation when it overtook the first shell (e.g., Fleischer et al. 1992; Schirrmacher et al. 2003).

6. SUMMARY AND CONCLUSIONS

V2362 Cyg was a most unusual and possibly unique object (Table 5). Only V1493 Aql showed a similar light curve and it was not observed with as much time regularity or with as many instruments as V2362 Cyg. It apparently experienced a second ejection that was moving faster than the first; the line widths tripled as the optical light curve approached its maximum just before dust formed. The X-ray flux reached a broad peak about 100 days after dust formation. During the second brightening, the spectrum evolved from an early nebular phase to an early post-maximum low excitation spectrum. Dust formation may have been triggered as the expanding shell from the second ejection interacted with the ejecta from the first one.

This work was supported in part by The Aerospace Corporation's Independent Research and Development program. We thank Daryl Kim, Ralph Ford, and Trishana Prater of the Aerospace Corporation for assistance in obtaining and reducing the IRTF data. We also thank IRTF telescope operators David Griep, William Golisch, and Paul Sears, as well as Lick telescope operators Kris Miller and Keith Baker. This work is based (in part) on observations made with the *Spitzer Space Telescope*, which is operated by the Jet Propulsion Laboratory, California Institute of Technology (CalTech) under a contract with NASA. Support for this work was provided by NASA through an award issued by JPL/Caltech. We acknowledge with thanks the variable star observations from the AAVSO International Database contributed by observers worldwide and used in this research. J.P.O. and K.P. acknowledge support from the Science and Technology Facilities Council (STFC) and are grateful to the *SWIFT* PI Prof. Neil Gehrel for his support of this observation campaign. We also thank David Dearborn for informative discussions about TNRs and Angela Speck for useful discussions about dust emission. Sumner Starrfield acknowledges NSF and NASA grants to Arizona State University. J.-U.N. gratefully acknowledges support provided by NASA through Chandra Postdoctoral Fellowship grant PF5-60039 awarded by The *Chandra* X-Ray Center, which is operated by the Smithsonian Astrophysical Observatory for NASA under contract NAS8-03060.

REFERENCES

Allamandola, L. J., Tielens, A. G. G. M., & Barker, J. R. 1985, ApJ, 290, L25
Bode, M. F., & Evans, A. 1989, Classical Novae (London: Wiley)
Bonifacio, P., Selvelli, P. L., & Caffau, E. 2000, A&A, 356, L53
Burrows, D. N., et al. 2005, Space Sci. Rev., 120, 165
Buscombe, W., & de Vaucouleurs, G. 1955, Obs., 75, 170
Buss, R. H., Tielens, A. G. G. M., & Snow, T. 1991, ApJ, 372, 281
Cushing, M. C., Vacca, W. D., & Rayner, J. T. 2004, PASP, 116, 362
Della Valle, M., & Livio, M. 1995, ApJ, 452, 704
Dobrotka, A., Friedjung, M., Retter, A., Hric, L., & Novak, R. 2006, A&A, 448, 1107
Fleischer, A. J., Gauger, A., & Sedlmayr, E. 1992, A&A, 266, 321
Gillett, F. C., Forrest, W. J., & Merrill, K. M. 1973, ApJ, 183, 87
Hernanz, M., Ferri, C., & Sala, G. 2007, ATel, 1226
Hernanz, M., & José, J. 2002, AIP Conf. Proc. 637, Classical Nova Explosions (New York: AIP)
Kahabka, P., & van den Heuvel, E. P. J. 1997, ARA&A, 35, 69
Kimeswenger, S., Dalnodar, S., Knapp, A., Schafer, J., Unterguggenberger, S., & Weiss, S. 2008, A&A, 479, L51
Kraft, R. P., Burrows, D. N., & Nousek, J. A. 1991, ApJ, 374, 344
Lynch, D. K., Rudy, R. J., Venturini, C. C., Mazuk, S., & Puetter, R. C. 2001, AJ, 122, 2013
Lynch, D. K., Russell, R. W., Kim, D., Sitko, M. L., & Brafford, S. 2006, IAU Circ., 8785
Lynch, D. K., Wilson, J. C., Rudy, R. J., Venturini, C. C., Mazuk, S., Miller, N. A., & Puetter, R. C. 2004, AJ, 127, 1089
Mazuk, S., Rudy, R. J., Lynch, D. K., Venturini, C. C., Puetter, R. C., & Perry, R. B. 2006, IAU Circ., 8731
Nakano, S., Nishimura, H., Miles, R., & Yamaoka, H. 2006, IAU Circ., 8697
Ness, J.-U., Schwarz, G. J., Retter, A., Starrfield, S., Schmitt, J. H. M. M., Gehrels, N., Burrows, D., & Osborne, J. P. 2007, ApJ, 663, 505
Rayner, J. T., Toomey, D. W., Onaka, P. M., Denault, A. J., Stahlberger, W. E., Vacca, W. D., Cushing, M. C., & Wang, S. 2003, PASP, 115, 362
Rudy, R. J., Dimpfl, D. L., Lynch, D. K., Mazuk, S., Venturini, C., Wilson, J. C., Puetter, R. C., & Perry, R. B. 2003, ApJ, 596, 1229
Rudy, R. J., Erwin, P., Rossano, G. S., & Puetter, R. C. 1991, ApJ, 383, 344
Russell, R. W., Rudy, R. J., & Lynch, D. K. 2006, IAU Circ., 8710
Schirrmacher, V., Woitke, P., & Sedlmayr, E. 2003, A&A, 404, 267
Sloan, G. C., et al. 2007, ApJ, 664, 1144
Steeghs, D., Greimel, R., Drew, J., Irwin, M., Gaensicke, B., Groot, P., & Knigge, C. 2006, ATel, 795
Venturini, C. C., Rudy, R. J., Lynch, D. K., Mazuk, S., & Puetter, R. C. 2004, AJ, 128, 405
Williams, P. M., Longmore, A. J., & Geballe, T. R. 1996, MNRAS, 279, 804